Computational Study of the Reaction of Fluorine Atom with Acetone

Yuzhen Li, Hui Li, Hua Hou, and Baoshan Wang*

College of Chemistry and Molecular Sciences, Wuhan University, Wuhan 430072, People's Republic of China

Received: December 29, 2004; In Final Form: February 11, 2005

The reaction of $F(^2P)$ with acetone has been studied theoretically using ab initio quantum chemistry methods and transition state theory. The potential energy surface was calculated at the G3MP2 level using the MP2/6-311G(d,p) optimized structures. Additionally, to ensure the accuracy of the calculations, optimizations with either larger basis set (e.g., MP2/G3MP2Large) or higher level electron correlation [e.g., CCSD/6-311G(d,p)] were also performed. It has been revealed that the $F + CH_3C(O)CH_3$ reaction proceeds via two pathways: (1) the direct hydrogen abstraction of acetone by F gives the major products $HF + CH_3C(O)CH_2$; (2) the addition of F atom to the >C═O double bond of acetone and the subsequent C−C bond cleavage gives the minor products $CH_3 + CH_3C(O)F$. All other product channels are of no importance due to the occurrence of significant barriers. Both abstraction and addition appear to be barrierless processes. Variational transition state model and multichannel RRKM theory were employed to calculate the temperature- and pressure-dependent rate constants and branching ratios. The predicted rate constants for the abstraction channel and the yields of $HF + CH_3C(O)CH_3$ and $CH_3 + CH_3C(O)F$ are both in good agreement with the experimental data at 295 K and 700 Torr. A negative temperature dependence of the overall rate constants was predicted at temperatures below 500 K.

I. Introduction

Ketones, notably acetone, represent an important class of oxygenated volatile organic compounds (VOCs). They are emitted into the atmosphere from a variety of anthropogenic and natural sources. In addition, atmospheric oxidation of volatile hydrocarbons constitutes a significant source of various ketones.[1,2] Solar photolysis and reactions with radicals (e.g., OH, Cl, F, O) play important roles in the tropospheric chemical degradation of ketones.[3]

Kinetic and mechanistic information on OH, Cl, and O initiated oxidation of acetone has been subject to numerous experimental and theoretical studies.[4−6] Rate constants for these reactions have been measured using various experimental techniques over a certain range of temperatures and pressures. In contrast, investigation on the reaction of F atom with acetone is very scarce. In the troposphere, F-containing compounds such as hydrofluorocarbons (HFCs), SF_6, and FCO_2 can be bombarded by intense ultraviolet or ionizing radiations, which break them down into free fluorine atoms.

Mechanistically, there is only one study reported by Nielsen and co-workers in 2001.[7] Using a FTIR−smog chamber system at 295 K and 700 Torr, they found that the reaction of F with $CH_3C(O)CH_3$ proceeds via H-atom abstraction (R1a) and displacement (addition−elimination, R1b) mechanisms:

$$F + CH_3C(O)CH_3 \rightarrow HF + CH_3C(O)CH_2 \quad (R1a)$$

$$F + CH_3C(O)CH_3 \rightarrow CH_3 + CH_3C(O)F \quad (R1b)$$

(R1a) is the major channel with a yield of 92% ± 3%, while (R1b) is the minor channel with a yield of 8% ± 1%. An upper limit of <2% was established for the yield of CH_3F, which is produced in another thermodynamically feasible channel:

$$F + CH_3C(O)CH_3 \rightarrow CH_3F + CH_3CO \quad (R1c)$$

Kinetically, there is only one relative rate measurement reported by Smith et al. in 1977.[8] In a flowing afterglow apparatus, the room-temperature rate constant for reaction R1a was measured relative to the $F + CH_4$ reaction by comparing HF infrared chemiluminescence.

$$F + CH_4 \rightarrow HF(X, v = 1-3) + CH_3 \quad (R2)$$

A value of 1.6 was obtained for the abstraction reaction (R1a). Using the well-established absolute rate constant for $k_2 = (6.24 \pm 0.94) \times 10^{-11}$ cm^3 molecule^{-1} s^{-1},[9] $k_{1a} = (10 \pm 1) \times 10^{-11}$ cm^3 molecule^{-1} s^{-1} could be deduced at $T = 295$ K.

In the consideration of atmospheric importance of the reaction between F and acetone, a computational study is worthwhile, not only to gain insight into the reaction mechanism but also to simulate its kinetic behavior over a wide range of temperatures and pressures. In this work, we report the reaction mechanism of the $F + CH_3C(O)CH_3$ reaction by calculating the potential energy surface (PES) including all possible product channels. Moreover, the ab initio data were employed to calculate the absolute rate constants as a function of temperature and pressure.

II. Computational Methods

The ab initio calculations were performed using the Gaussian03 suite of programs.[10] Only the potential energy surface in its ground electronic state was explored in this work. Initially, the geometries were optimized at the MP2 level using analytic gradients with only valence orbitals active. The basis set used in the MP2 calculations was the standard 6-311G(d,p).[11] The

* Corresponding author. Fax: 86-27-68754067. E-mail: wangb@chem.whu.edu.cn.

10.1021/jp044086k CCC: $30.25
Published on Web 03/19/2005

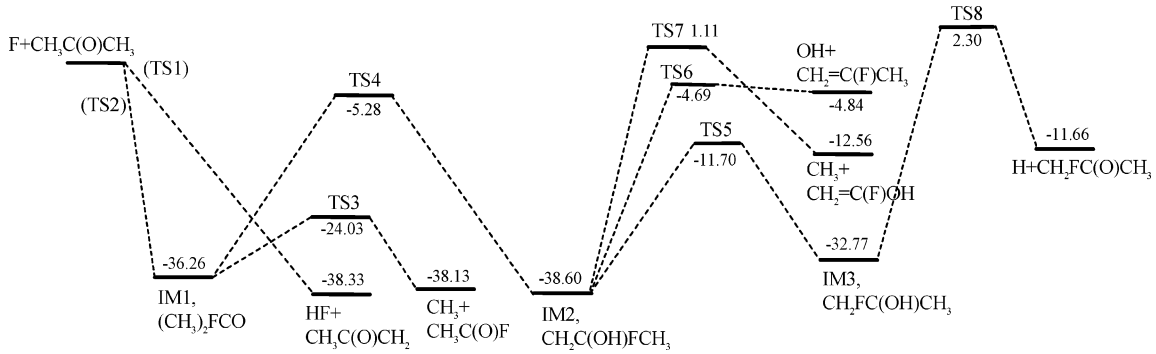

Figure 1. Schematic profiles of the most important reaction paths involved in the F + $CH_3C(O)CH_3$ reaction. The numbers indicated correspond to the relative energies (in kcal/mol) calculated at the G3MP2 level including ZPE corrections.

stationary points were characterized as a minimum or a transition state (one imaginary frequency) by determination of harmonic vibrational frequencies using analytic second derivatives at the MP2/6-311G(d,p) level of theory. The zero-point energy (ZPE) was determined by using the calculated harmonic frequencies scaled by 0.95.[12]

To check the influence of basis set and higher level electron correlation on the MP2/6-311G(d,p) optimized geometric parameters, we performed geometric optimization with two alternative methods. One is MP2 theory but with a more flexible basis set, namely G3MP2Large,[13] which corresponds to 6-311++G(2df,2p) for [H,C,O,F]-containing system of our interest. The other is coupled-cluster theory with single and double excitations (CCSD)[14] using the 6-311G(d,p) basis set. Both optimizations are very time-consuming, so only the species involved in the most important pathways (see Figure 1) were considered.

G3MP2 theory was employed at the MP2/6-311G(d,p) optimized geometries to calculate relative energies. The G3MP2 scheme was detailed elsewhere,[13] and only a brief description is given here. Single-point-energy evaluations were performed at the QCISD(T)/6-31G(d) (E_1), MP2/6-31G(d) (E_2), and MP2/G3MP2Large (E_3) levels of theory, respectively. The combination of these three energies gives an approximation to the total energy at the QCISD(T)/G3MP2Large level. The high-level correction (HLC) takes into account the remaining deficiencies in the above energy calculations. The ΔE_{HLC} (in millihartrees) is $-4.471n_\alpha - 4.808n_\beta$ for molecules and $-2.021n_\alpha - 7.324n_\beta$ for atoms. n_α and n_β are the number of α and β valence electrons, respectively, with $n_\alpha \geq n_\beta$. The spin−orbital correction (ΔE_{SO}) was made for atomic species. Finally, the G3MP2 total energy was calculated as follows:

$$E_0(\text{G3MP2}) = E_1 + (E_3 - E_2) + \Delta E_{HLC} + \Delta E_{SO} + \text{ZPE}$$

It is noted that the sum of ($\Delta E_{HLC} + \Delta E_{SO}$) contributes −1.03 kcal/mol to the relative energies with respect to the initial reactants [F + $CH_3C(O)CH_3$]. All Hartree−Fock (HF) and post-HF calculations were performed using the unrestricted methodology for both open-shell and closed-shell species. Alternatively, rather than the regular MP2, the spin-projected Møller−Plesset theory through the second order (PMP2) was used in the calculations of E_2 and E_3 in order to annihilate spin contamination.[15] However, this alternation does not have significant impact on the calculated relative energies. The good performance of G3MP2 theory in the calculation of both barrier height and heat of reaction has been outlined elsewhere.[13] In our previous calibration calculation, G3 theory gives an average absolute deviation of only 1.1 kcal/mol for barrier heights of a test set that consists of 39 well-known radical reactions.[16] *All activation and reaction energies reported include zero-point-energy corrections.*

Variational transition state theory (VTST) and multichannel Rice−Ramsperger−Kassel−Marcus (RRKM) calculations have been carried out for the total and individual rate constants and the branching ratios for various product channels. The formulas are listed in Note S1 as Supporting Information.

III. Results and Discussion

III.1. Reaction Mechanism. Three types of mechanisms have been revealed for the F + $CH_3C(O)CH_3$ reaction, namely, direct hydrogen abstraction, addition/elimination, and S_N2 displacement. For clarity, the most important paths, which involve relatively low barriers, are schematically summarized in Figure 1. The corresponding geometries are shown in Figure 2. The relative energies at various levels of theory are listed in Table 1. Harmonic vibrational frequencies for the reactants, transition states, and intermediates, which will be used in the following kinetic simulation, are summarized in Table 2.

Figure 3 shows the reaction paths with high barriers. The corresponding structures and energies are given as Supporting Information (Figure S1 and Table S1). Although all of them are exothermic channels, all of them are kinetically forbidden. These paths cannot be important under normal experimental or atmospheric conditions and will not be discussed further. A detailed discussion on the mechanism as shown in Figure 1 is given as follows.

III.1.1. Abstraction Channel. Direct hydrogen abstraction reaction proceeds via a transition state (TS1). As shown in Figure 2, TS1 is obviously an early barrier. The breaking CH bond is stretched by only about 0.04 Å (ca. 3.6% of the equilibrium CH bond). The forming HF bond is 1.407 Å, which is 0.494 Å longer than that of the HF molecule. The calculated heat of reaction at 0 K (−38.3 kcal/mol) is in good agreement with the experimental value (−38.7 kcal/mol).[17] Presumably, the product generated in a highly exothermic reaction via an early barrier might be internally excited. In fact, the HF molecules were observed experimentally to be vibrationally excited even with populations inversed, that is, $v_1/v_2/v_3 = 0.33/0.50/0.17$. According to the highest vibrational quantum number ($v = 3$) and the frequency of HF (4138 cm^{-1} = 11.8 kcal/mol), it was estimated that most of the available energy in the abstraction is deposited as the vibrational energy of HF molecules. At the MP2/6-311G(d,p) level, the barrier for TS1 is 1.2 kcal/mol. However, TS1 lies below the reactants at the G2MP2 level by −2.8 kcal/mol, which implies that the abstraction is actually a barrierless process. More details on the minimum energy reaction path (MERP) for the abstraction will be given in section III.2.

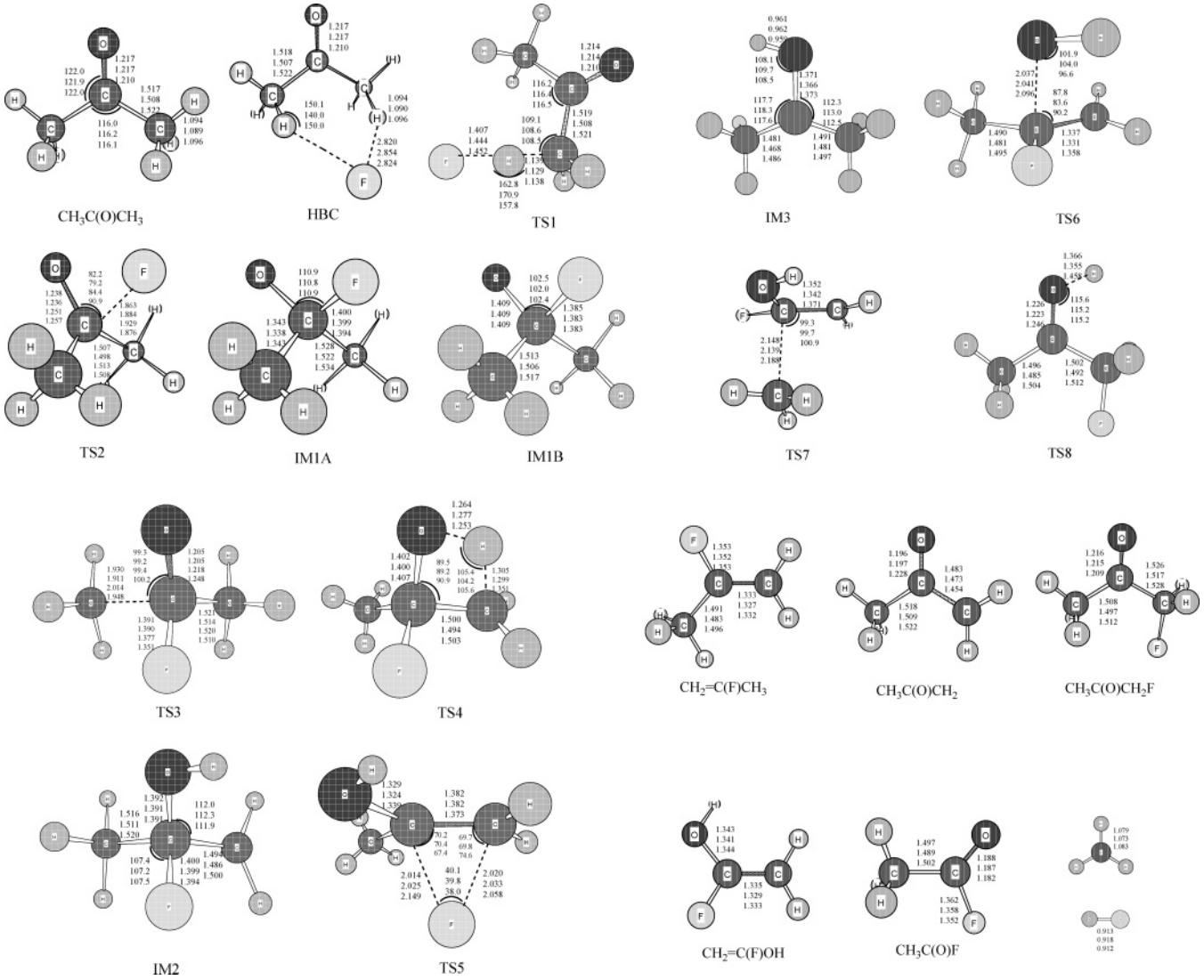

Figure 2. UMP2/6-311G(d,p) optimized geometries of various species involved in the most important reaction paths of the F + $CH_3C(O)CH_3$ reaction (corresponding to the stationary points in Figure 1). The second and third entries correspond to the optimized geometric parameters at UMP2/G3MP2Large and CCSD/6-311G(d,p) levels of theory, respectively. In the case of TS2 and TS3, the fourth entries are optimized at the CAS(9,7)/6-311G(d,p) level. Bond distances are in angstroms and angles are in degrees.

It is worth noting that TS1 is different from the abstraction transition state for the OH + $CH_3C(O)CH_3$ reaction. In the latter, two transition states were found.[4] One is similar to TS1. The other involves a relatively strong six-membered-ring hydrogen-bonding complex formed between H of OH and O of carbonyl (C═O) group of acetone. For the F + $CH_3C(O)CH_3$ reaction, however, there is no way to form such a bond so that only one transition state was located. In addition, we did check the structure with "F−H−C−C═O" in the plane. However, such a structure involves two imaginary frequencies and thus is not a real transition state. On the other hand, as shown in Figure 2, a very weak interaction occurs between F and the two methyl groups of acetone (see the structure labeled as HBC).

III.1.2. Addition Channel. F atom can add to the >C═O double bond of acetone, forming the F-substituted alkoxy radical adduct (IM1, see Figure 2). The corresponding transition state for addition is shown as TS2. The reacting CO bond is stretched to 1.238 Å, while the forming CF bond is 1.863 Å. By comparing the geometric parameters of TS1 with those of IM1, it is known that TS2 is an early barrier. At the MP2/6-311G(d,p) level, the barrier is 11.5 kcal/mol. However, this barrier is reduced significantly to be negative (−0.39 kcal/mol) at the higher G3MP2 level. This implies that the addition of F to $CH_3C(O)CH_3$ proceeds on an attractive potential energy surface and is free of any barrier.

Within C_s symmetry, IM1 has two distinct structures, which belong to $^2A''$ (IM1A) and $^2A'$ (IM1B) electronic states, respectively. The only discernible difference between these two structures is the length of the CO bond. The $^2A'$ structure has a slightly longer CO bond. It is known that such a difference results from the orientation of the lone-pair electrons on oxygen atom (e.g., $^2A'$ with in-the-plane lone pair and $^2A''$ with out-of-plane lone pair). Energetically, IM1A is more stable than IM1B.

III.1.3. Elimination and Isomerization Channels. Starting from the initial adduct IM1, the formation of CH_3 + $CH_3C(O)F$ proceeds via a simple CC bond cleavage. Transition state TS3 is obviously a late barrier. The breaking CC bond is stretched to 1.930 Å. The CO bond distance is reduced to 1.205 Å, leading to the carbonyl C═O bond in $CH_3C(O)F$. The barrier for TS3 is below the F + $CH_3C(O)CH_3$ reactants by 24.0 kcal/mol, and it is the lowest decomposition barrier of IM1. It is conceivable that there is a certain yield for CH_3 + $CH_3C(O)F$ channel in the F + $CH_3C(O)CH_3$ reaction, as observed in FTIR−smog chamber experiments.[7] Quantitative calculations of rate constant and yield as detailed below provide numerical evidence for the

TABLE 1: Zero-Point Energies (ZPE, in kcal/mol) and Relative Energies (ΔE_i, with ZPEs Scaled by 0.95, in kcal/mol) of Various Species Involved in the "Important Paths" of the F + $CH_3C(O)CH_3$ Reaction[a]

species	$<S^2>$[b]	ZPE	ΔE_1	ΔE_2	ΔE_3	ΔE_4	ΔE_5	ΔE_6	experimental[c]
F + $CH_3C(O)CH_3$		53.06	0	0	0	0	0	0	
HBC	0.752	53.26	−3.33	−1.59	−0.61	−1.63	−1.04	−1.59	
TS1	0.771	51.05	1.24	−2.79	1.89	−2.33	1.50	−2.36	
HF + $CH_3C(O)CH_2$		51.17	−32.54	−38.33	−37.56	−38.52	−31.38	−39.72	−38.7 ± 2.9
TS2	0.920	53.88	11.53	−0.39	9.96	0.37	5.84	−0.05	
IM1A ($^2A''$)	0.758	55.41	−31.10	−36.26	−33.54	−36.23	−30.51	−36.30	
IM1B ($^2A'$)	0.756	55.78	−20.80	−25.04	−22.85	−25.03	−20.30	−25.07	
TS3	0.851	53.45	−16.54	−24.03	−21.04	−23.98	−14.60	−24.06	
CH_3 + $CH_3C(O)F$		50.06	−38.49	−38.13	−41.36	−38.10	−31.75	−38.13	−37.6, −39.3
TS4	0.793	52.43	0.19	−5.28	−3.85	−5.36	3.97	−5.50	
IM2	0.762	54.64	−36.61	−38.60	−41.38	−38.64	−31.03	−38.64	
TS5	0.788	54.99	−2.35	−11.70	−12.30	−11.99	3.93	−12.93	
IM3	0.762	56.16	−28.84	−32.77	−34.89	−32.97	−23.85	−32.80	
TS6	0.914	53.68	8.46	−4.69	2.43	−3.86	5.54	−4.82	
OH + CH_2=$CFCH_3$		51.28	1.13	−4.84	−2.51	−4.83	2.29	−4.89	
TS7	0.956	52.24	10.88	1.11	4.84	1.31	11.13	0.95	
CH_3 + CH_2=CFOH		49.90	−9.34	−12.56	−14.55	−12.56	−4.01	−12.62	
TS8	0.885	50.47	10.29	2.30	4.56	2.62	12.51	2.37	
H + $CH_3C(O)CH_2F$		48.91	−12.32	−11.66	−15.82	−11.30	−1.52	−11.31	

[a] ΔE_1, ΔE_2, ΔE_3, ΔE_4, ΔE_5, and ΔE_6 represent the relative energies calculated at the MP2/6-311G(d,p), G3MP2//MP2/6-311G(d,p), MP2/G3MP2Large, G3MP2//MP2/G3MP2Large, CCSD/6-311G(d,p), and G3MP2//CCSD/6-311G(d,p) levels of theory, respectively. [b] Expectation values of S^2 of the Hartree−Fock wave functions. The deviation of these values from the exact value of 0.75 for doublets reflects the extent of spin contamination. [c] Experimental heats of reaction were calculated using the experimental enthalpies of formation for the relevant species taken from ref 17.

TABLE 2: Vibrational Frequencies (in cm^{-1}) and Moments of Inertia (in amu·$bohr^2$) Used in the Transition State Theory and Multichannel RRKM Calculations

species	I_a, I_b, I_c	I_r[a]	frequencies[c]
CH_3COCH_3	179.5, 211.3, 368.4	11.08, 10.34	*79*, *139*, 377, 482, 534, 804, 889, 906, 1091, 1121, 1254, 1395, 1406, 1482, 1486, 1492, 1507, 1788, 3075, 3080, 3158, 3163, 3204, 3205
HBC	294.4, 997.9, 1103.3		22, 23, 57, 60, 159, 380, 485, 535, 805, 887, 903, 1093, 1125, 1254, 1395, 1406, 1483, 1487, 1492, 1508, 1787, 3078, 3083, 3163, 3168, 3206, 3207
TS1	234.0, 694.7, 856.9 (*236.9*, *707.5*, *871.0*)[b]	21.05, 3.88, 10.95, 123.8	869i, *39*, *89*, *140*, *188*, 358, 479, 525, 799, 874, 899, 1053, 1114, 1195, 1309, 1338, 1407, 1453, 1484, 1497, 1736, 1917, 3086, 3128, 3172, 3211, 3219
TS2	338.0, 376.1, 437.2	11.27, 10.93	929i, *125*, *198*, 223, 280, 401, 456, 533, 817, 892, 951, 1042, 1099, 1284, 1403, 1419, 1474, 1479, 1488, 1506, 1603, 1488, 1506, 1603, 3189, 3227, 3229
TS3	346.3, 380.9, 401.0		788i, 141, 231, 269, 283, 420, 525, 585, 714, 758, 802, 978, 1021, 1140, 1177, 1408, 1450, 1467, 1498, 1501, 1714, 3103, 3139, 3200, 3230, 3312, 3323
TS4	305.6, 349.1, 404.9		2345i, 254, 317, 361, 397, 475, 527, 683, 871, 900, 960, 994, 1033, 1166, 1177, 1265, 1329, 1434, 1446, 1503, 1508, 2115, 3094, 3170, 3191, 3199, 3300
IM2	346.3, 357.0, 365.8		185, 249, 322, 366, 415, 441, 497, 550, 591, 813, 919, 982, 1005, 1126, 1235, 1285, 1385, 1435, 1477, 1503, 1510, 3096, 3197, 3204, 3216, 3344, 3869
TS5	305.8, 406.4, 465.4		464i, 126, 159, 360, 415, 471, 495, 573, 681, 829, 900, 1014, 1053, 1063, 1249, 1407, 1464, 1486, 1504, 1507, 1746, 3098, 3191, 3225, 3238, 3362, 3851
IM3	247.3, 468.1, 593.4		89, 150, 204, 370, 379, 429, 588, 824, 983, 987, 1030, 1062, 1181, 1274, 1381, 1399, 1441, 1464, 1491, 1516, 1523, 3052, 3086, 3141, 3168, 3186, 3886
TS6	346.1, 398.3, 436.8		636i, 184, 197, 237, 287, 397, 455, 491, 749, 795, 872, 898, 986, 1039, 1072, 1338, 1419, 1459, 1489, 1505, 1720, 3102, 3196, 3226, 3234, 3354, 3849
TS7	350.4, 408.0, 414.4		973i, 131, 147, 239, 250, 448, 474, 538, 609, 630, 642, 729, 914, 980, 991, 1208, 1407, 1448, 1455, 1457, 1625, 3127, 3236, 3297, 3303, 3352, 3904
TS8	220.9, 459.5, 649.7		2913i, 114, 147, 229, 265, 405, 491, 527, 779, 839, 881, 1018, 1125, 1133, 1275, 1305, 1402, 1417, 1473, 1487, 1492, 1864, 3028, 3071, 3155, 3161, 3220

[a] Moments of inertia for free rotors. [b] Moments of inertia extrapolated from the G2MP2 minimum energy reaction path (see text and Figure 4 for details). These three values were used in the TST calculation. [c] "i" represents imaginary frequency.

experimental observation. Moreover, the calculated heat of reaction at 0 K (−38.1 kcal/mol) is in agreement with the experimental value (in the range of −37.5 and −39.3 kcal/mol) as well.[17]

IM1 undergoes isomerization via a 1,3-H shift transition state TS4, with one of the hydrogen atoms of the methyl group in IM1 migrating to the terminal oxygen atom. The isomer IM2 can be seen as a substituted methyl radical. Its energy is close to that of IM1. The isomerization barrier for TS4 lies 5.3 kcal/mol below the reactants, which is 18.8 kcal/mol higher than that for TS3. Such a big difference in barriers indicates that the isomerization is only a minor channel in comparison with the CC bond fission decomposition.

Subsequent unimolecular reactions of IM2 were investigated for completeness. Interestingly, the three-center F-migration path involves the lowest barrier (−11.7 kcal/mol), leading to another intermediate, IM3. The other two reactions are simple bond fission processes, forming fluorinated alkene molecules. While the energy of TS6 is 4.7 kcal/mol lower than that of the reactants, the energy of TS7 is slightly higher than that of the reactants. The intermediate IM3 is stable both kinetically and thermodynamically. The cleavage of OH bond to form fluoroacetone involves the lowest barrier (TS8). However, the energy of TS8 is already 2.3 kcal/mol higher than that of the reactants. Experimentally, no fluoroacetone has ever been observed.[7]

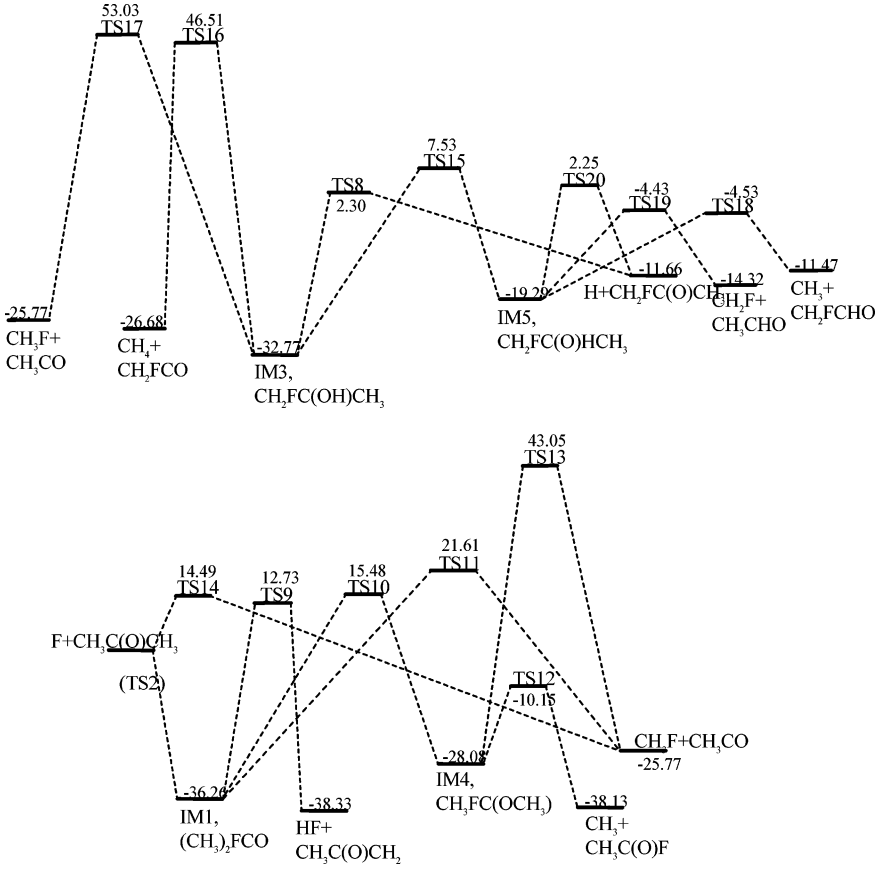

Figure 3. Potential energy profiles for high energy reaction channels in F + $CH_3C(O)CH_3$ reaction. The numbers correspond to the G3MP2 relative energies (in kcal/mol) with respect to the reactants. Note that this figure together with Figure 1 gives the complete reaction mechanism investigated in this study for the F + $CH_3C(O)CH_3$ reaction.

III.1.4. Basis Set and Electron Correlation Dependence. As can be seen in Figure 2, the MP2/G3MP2Large optimized structural parameters show some differences from those of the MP2/6-311G(d,p) values, especially for the transition states. Overall, only the reacting bonds are affected by the larger basis set. For instance, it appears that the MP2/G3MP2Large optimization leads to either the slightly longer breaking bonds in TS1(F···H) and TS2(C···F) or the slightly shorter C···C bonds (TS3, TS7). More significantly, the reacting FHC angle in TS1 is enlarged to 170.9° in comparison with 162.8°. As can be seen in Table 1, the relative energies obtained at the MP2/6-311G(d,p) and the MP2/G3MP2Large levels have significant differences. However, almost identical energies are obtained at the G3MP2 level with the geometries at both levels.

A similar trend has been found for the CCSD/6-311G(d.p) optimized structural parameters. For the stable minima (reactants, intermediates, and products), the geometries have only a little change. For the transition states, it appears that the breaking bonds become slightly longer, which means that the transition states tend to be more reactant-like. For example, the reacting F···H (TS1), C···F (TS2), C···C (TS3), C···H (TS4), C···F (TS5), C···O (TS6), C···C (TS7), and O···H (TS8) bonds are elongated further by 0.05−0.1 Å systematically with respect to the MP2/6-311G(d,p) optimized data. The relative energies at the CCSD/6-311G(d,p) level are also quite different from those at the MP2/6-311G(d,p) level, as shown in Table 1. However, the G3MP2 calculations at the CCSD/6-311G(d,p) geometries give relative energies nearly identical with those at the MP2/6-311G(d,p) geometries.

Therefore, it is concluded that the G3MP2 calculations on the relative energies are not sensitive to the geometries used. Among the six levels of theory in Table 1, the G3MP2 calculated heats of reaction show the best agreement with the experimental values. Together with our previous calibration calculations for the barrier heights,[16] the calculated potential energy surface in this paper should be quantitatively good enough to be employed in the following kinetic simulation.

III.2. Kinetic Simulation. Principally, the kinetic calculation is straightforward using transition state theory (TST) and multichannel RRKM theory on the basis of ab initio energetics, frequencies, and moments of inertia. In fact, these methods have been successfully used to deal with many complex-forming bimolecular reactions.[18] However, for the F + $CH_3C(O)CH_3$ reaction of interest, such a calculation might not be so straightforward because both the abstraction path and the entrance of the addition reaction are essentially barrierless. A variational treatment is required for such processes.

Thus intrinsic reaction coordinate (IRC)[19] calculations were first performed for the abstraction path at the MP2/6-311G(d,p) level. Vibrational frequencies and moments of inertia were also obtained for each point along the IRC path at the same level of theory with one imaginary frequency projected out. As shown in Table 1, the MP2/6-311G(d,p) energies are not accurate enough for kinetic analysis. Therefore, the energy of each point was calculated at the G3MP2 level (excluding ZPE). Profiles of the relative energies are shown in Figure 4. Obviously, the G3MP2 profile is significantly different from the MP2/6-311G(d,p) profile. While the latter has a maximum (ΔE = 3.2 kcal/mol) at $s = 0$, the maximum point along the former moves back to the reactant side at $s = -0.5$ with a value of $\Delta E = 0.29$ kcal/mol. The rate constants, $k(T,s)$, were calculated at each point along the G3MP2 profile and then were minimized

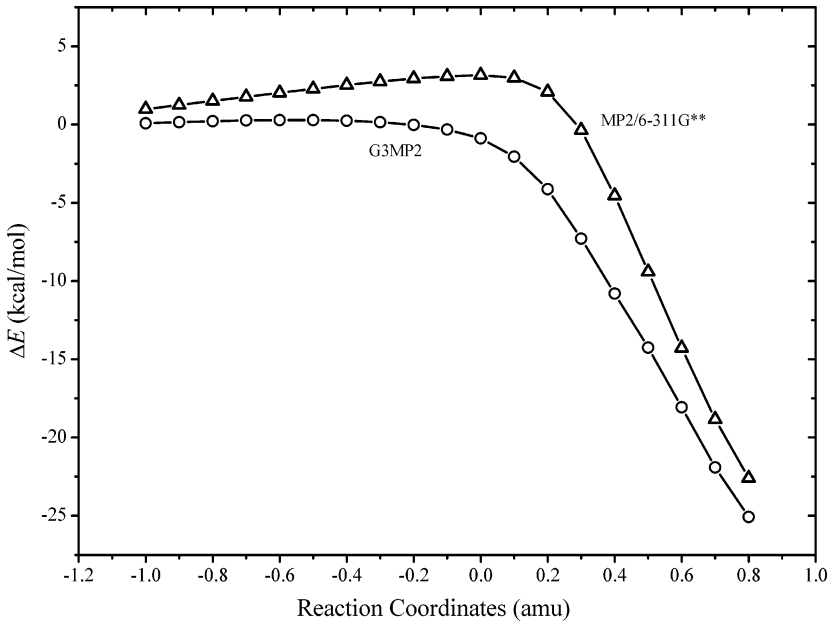

Figure 4. Calculated minimum energy reaction path for direct hydrogen abstraction of $CH_3C(O)CH_3$ by F atom at MP2/6-311G(d,p) (triangles) and G3MP2 (circles) levels, respectively. The *X*-axis represents reaction coordinates, *s*, in units of amu·bohr$^{-1/2}$. The *Y*-axis shows the relative energy to the reactants (F + CH_3COCH_3). The maximum of the MP2/6-311G(d,p) profile is at $s = 0$, which corresponds to transition state TS1. The maximum of the G3MP2 profile occurs between $s = -0.5$ and $s = -0.6$.

with respect to *s* to obtain $k(T)$ variationally. It turns out that the minimum of $k(T,s)$ always locates at the reactant side, namely, $s \leq -1.0$ with a relative energy of $\Delta E \leq 0.082$ kcal/mol, over a temperature range of 200−2000 K. This implies that the variational effect is nearly constant and the contribution of the potential energy (ΔE) to $k(T)$ is negligible since $\exp(-\Delta E/RT) \approx 1$. Therefore, a "loose" transition state model was assumed for the abstraction for simplicity. The barrier height was set to be zero, and the frequencies are the same as those of acetone. To account for the transitional vibrational modes, four free one-dimensional internal rotors were used. The reduced moments of inertia (equal to the nonzero eigenvalues of the kinetic energy matrix) were obtained using Schlegel's method.[20] It should be noted that, among four internal rotors, two are for transitional modes between F and acetone and the other two are for CH_3 internal rotation. Although one CH_3 might be perturbed by an F atom during abstraction, the interaction between F and CH_3 is so weak that CH_3 could rotate freely. Therefore, the free-rotor approximation should be reasonable. In addition, two free internal rotors (i.e., two CH_3 rotors) were also considered for acetone. The electronic partition function of F atom was calculated by $Q_e[F(^2P)] = 4 + 2\exp(-581/T)$. A statistical factor of 6 was used to account for the degeneracy of abstraction.

RRKM theory was employed for the addition path. Two free internal rotors were considered for TS2 by taking into account the nearly free rotations of two methyl groups. The remaining transition states (TS3−TS8) are all tight transition states, and thus the RRHO (rigid-rotor harmonic oscillator) approximation was used for all normal modes. All product channels shown in Figure 1 were considered in the multichannel RRKM program. The details for the RRKM calculation are shown in the Supporting Information (Note S1). All the data required in the kinetic calculation are summarized in Table 2.

The rate constants were calculated at $P = 700$ Torr and $T = 200-2000$ K. The rate constants and thus branching ratios for H abstraction and formation of CH_3 + $CH_3C(O)F$ of most concern are shown in Figure 5. The numerical results are given in Table S2 as Supporting Information. It is noted that all the other product channels including the deactivation of various intermediates are negligible. The experimental rate constant at 295 K for the abstraction channel is $k_{abs} = (10 \pm 1) \times 10^{-11}$ cm^3 molecule^{-1} s^{-1}. The calculated value of 9.8×10^{-11} cm^3 molecule^{-1} s^{-1} is in good agreement with the experimental value. Moreover, the calculated yield of abstraction channel, $\Phi[HF+CH_3C(O)CH_2] = 0.93$, is also in good agreement with the experimental value (0.92 ± 0.03). The production of CH_3 + $CH_3C(O)F$ is always a minor channel. Its yield was estimated to be 0.069 at 295 K, which is in agreement with the experimental value (0.08 ± 0.01). More experimental data are required to validate the present theoretical results.

As shown in Figure 5, the rate constants show a weak negative temperature dependence below the temperature of 500 K. This prediction needs to be validated by new experimental data in the high-temperature region. It is worth noting that the negative temperature dependence has been observed for the analogous reaction between OH and acetone at temperatures below 300 K.[4] For convenience, the calculated rate constants have been fitted by the following empirical expression ($P =$ 700 Torr, $T = 200-2000$ K):

$$k_{tot} = (1.4 \pm 0.2)e^{(557\pm7)/T} + (12.2 \pm 0.3)e^{-(638\pm5)/T}$$

(in units of 10^{-11} cm^3 molecule^{-1} s^{-1})

Only the addition/elimination channels are relevant to pressure. At the high-pressure limit, the collisional deactivation of the initial adduct (IM1) will take over the decomposition. Because the addition is always a minor channel, the pressure dependence of the rate constants was not investigated. It is worth noting that $P = 700$ Torr is in the falloff region.

While it is confirmed that the reaction of F with acetone proceeds always via the major abstraction channel, the contribution from the addition/elimination process giving CH_3 and $CH_3C(O)F$ is small but discernible (ca. >5%). Moreover, this displacement mechanism might play a significant role especially at lower temperatures. For instance, the yield of CH_3 + $CH_3C(O)F$ is as large as 18.4% at 200 K, which indicates that

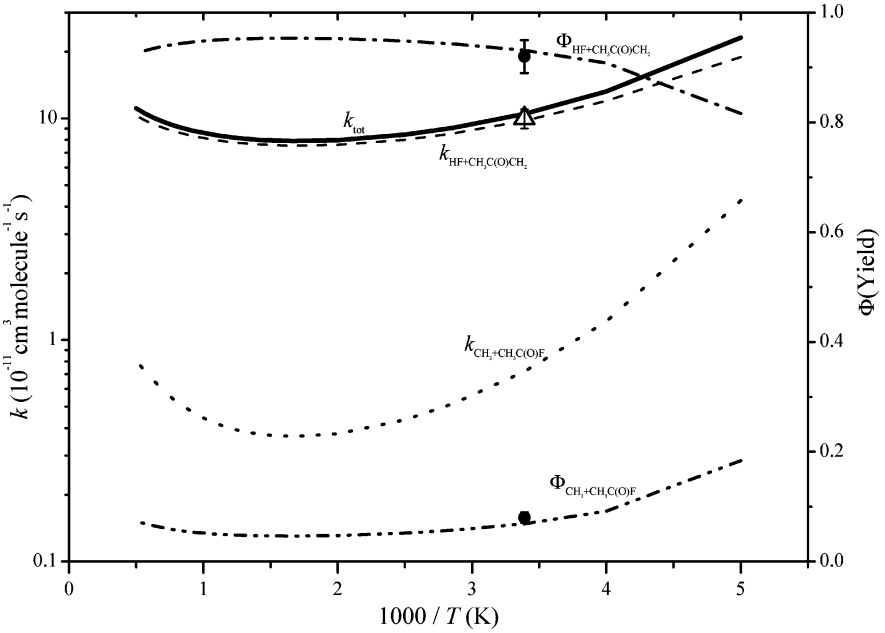

Figure 5. Calculated rate constants (left *Y*-axis) and yields of HF + $CH_3C(O)CH_2$ and CH_3 + $CH_3C(O)F$ (right *Y*-axis) at $P = 700$ Torr of helium. Solid line, k_{tot}: total rate constants. Dashed line, $k_{HF+CH_3C(O)CH_2}$: rate constants for the HF + $CH_3C(O)CH_2$ channel. Dotted line, $k_{CH_3+CH_3C(O)F}$: rate constants for the CH_3 + $CH_3C(O)F$ channel. Dot−dashed line,, $\Phi_{HF+CH_3C(O)CH_2}$: yield of the HF + $CH_3C(O)CH_2$ channel. Dot−dot−dashed line, $\Phi_{CH_3+CH_3C(O)F}$: yield of the CH_3 + $CH_3C(O)F$ channel. The open triangle is the experimental rate constant for the abstraction path at 295 K reported in ref 8. The filled circles represent the experimental yields of HF + $CH_3C(O)CH_2$ and CH_3 + $CH_3C(O)F$ in ref 7.

the production of CH_3 + $CH_3C(O)F$ could be important under atmospheric conditions.

III.3. Error Analysis. The possible errors in the present kinetic prediction lie in two aspects. First, the calculated potential barriers might be inaccurate from using a single-reference Hamilton for the open-shell system. The G3 serials of theory have an average uncertainty of around 1.0 kcal/mol for enthalpies of formation (for radical species, the uncertainty is slightly larger).[13] For a transition state, it has been shown that the average uncertainty is around 1.1 kcal/mol with maximum errors ranging from −2.7 to +3.5 kcal/mol in a test set of 39 well-known radical reactions.[16] As for the F + $CH_3C(O)CH_3$ reaction, fortunately, the barriers involved in the most important reaction paths are well separated. As can be seen from Figure 1, the huge barrier difference between TS3 and TS4 unambiguously leads to the conclusion that the formation of CH_3 + $CH_3C(O)F$ via TS3 is the dominant product channel.

It is noted that two key transition states, TS2 and TS3, involve serve spin contaminations, as indicated by the expectation values of S^2 in Table 1. The multiconfigurational SCF calculation[21] was performed for both species using an active space including nine electrons in seven orbitals, i.e., CAS(9,7), with the 6-311G(d,p) basis set. It turns out the contribution from the HF determinant is dominant with coefficients greater than 0.95 (e.g., 0.956 and 0.969 for TS2 and TS3, respectively). The optimized geometric structures are shown in Figure 2. It is evident that the CAS(9,7) parameters are in agreement with the MP2 and CCSD results.

Second, the treatment for the reaction entrance might be too crude. Both abstraction and addition pathways are governed by the multidimensional entrance potential surface. Such a surface should be highly attractive and is dominated by the long-range interaction between F atom and acetone. A "loose transition state" treatment is only for the purpose of simplicity. Evidently it cannot give a quantitative description of the entrance surface. Therefore, the amazing good agreement between the present theoretical data and the experimental data might be just a coincidence. More definitive computational work is needed to perform the first-principles kinetics of the present reaction.

IV. Conclusions

Ab initio calculation has been performed for the reaction of F atom with acetone. Both hydrogen abstraction and addition/elimination mechanisms were revealed. The major channel gives HF and $CH_3C(O)CH_2$ via abstraction. The minor channel proceeds via the addition of F atom to the double bond of acetone forming a fluorinated alkoxy radical intermediate. The subsequent decomposition gives CH_3 and $CH_3C(O)F$ via CC bond cleavage. It was confirmed that both abstraction and addition steps are essentially barrierless. All other channels are of no importance.

Kinetics analysis has also been done on the basis of ab initio data. A loose transition state approximation together with multichannel RRKM theory gives reasonable rate constants and thus branching ratios for the F + $CH_3C(O)CH_3$ reaction. The calculated rate constant for abstraction is in good agreement with the experimental value. The theoretical yields of HF + $CH_3C(O)CH_2$ and CH_3 + $CH_3C(O)F$ also support recent experimental observation. It is predicted that the overall rate constants have a negative temperature dependence at temperatures below 500 K.

Acknowledgment. This work was supported by A Foundation for the Author of National Excellent Doctoral Dissertation of the People's Republic of China (FANEDD, 200224).

Supporting Information Available: Figure S1 shows the structures of species involved in Figure 3. Table S1 gives the ZPEs, MP2/6-311G(d,p), and G3MP2 relative energies of the species involved in Figure 3. Table S2 summarizes the calculated rate constants for various product channels. Note S1 gives the details of the multichannel RRKM calculation. This material is available free of charge via the Internet at http://pubs.acs.org.

References and Notes

(1) Singh, H. B.; Kanakidou, M.; Crutzen, P. J.; Jacob, D. J. *Nature* **1995**, *378*, 50.

(2) Atkinson, R. *J. Phys. Chem. Ref. Data* **1997**, *26*, 215.

(3) Chatfield, R. B.; Gardner, E. P.; Calvert, J. G. *J. Geophys. Res.* **1987**, *92*, 4208.

(4) For the OH + $CH_3C(O)CH_3$ reaction, see: (a) Wollenhaupt, M.; Carl, S. A.; Horowitz, A.; Crowley, J. N. *J. Phys. Chem. A* **2000**, *104*, 2695. (b) Wollenhaupt, M.; Crowley, J. N. *J. Phys. Chem. A* **2000**, *104*, 6429. (c) Vasvari, G.; Szilagyi, I.; Bencsura, A.; Dobe, S.; Berces, T.; Henon, E.; Canneaux, S.; Bohr, F. *Phys. Chem. Chem. Phys.* **2001**, *3*, 551. (d) Calve, S. L.; Hitier, D.; Bras, G. L.; Mellouki, A. *J. Phys. Chem. A* **1998**, *102*, 4579. (e) Tyndall, G. S.; Orlando, J. J.; Wallington, T. J.; Hurley, M. D.; Goto, M.; Kawasaki, M. *Phys. Chem. Chem. Phys.* **2002**, *4*, 2189. (f) Vandenberk, S.; Vereecken, L.; Peeters, J. *Phys. Chem. Chem. Phys.* **2002**, *4*, 461. (g) Talukdar, R. K.; Gierczak, T.; McCabe, D. C.; Ravishankara, R. *J. Phys. Chem. A* **2003**, *107*, 5021. (h) Henon, E.; Canneaux, S.; Bohr, F.; Dobe, S. *Phys. Chem. Chem. Phys.* **2003**, *5*, 333. (i) Smith, I. W. M.; Ravishankara, A. R. *J. Phys. Chem. A* **2002**, *106*, 4798. (j) Turpin, E.; Fittschen, C.; Tomas, A.; Devolder, P. *J. Atmos. Chem.* **2003**, *46*, 1.

(5) For the Cl + $CH_3C(O)CH_3$ reaction, see: (a) Wallington, T. J.; Andino, J. M.; Ball, J. C.; Japar, S. M. *J. Atmos. Chem.* **1990**, *10*, 301. (b) Olsson, B.; Hallquist, M.; Ljungstrom, E.; Davidson, J. *Int. J. Chem. Kinet.* **1997**, *29*, 195. (c) Notario, A.; Mellouki, A.; LeBras, G..L. *Int. J. Chem. Kinet.* **2000**, *32*, 62.

(6) For the O + $CH_3C(O)CH_3$ reaction, see: (a) Ambidge, P. F.; Bradley, J. N.; Whytock, D. A. *J. Chem. Soc., Faraday Trans. 1* **1976**, *72*, 1870. (b) Mix, K. H.; Wagner, H. Gg. *Oxid. Commun.* **1983**, *5*, 321. (c) Roscoe, J. M. *Can J. Chem.* **1986**, *64*, 1458. (d) Lee, J. H.; Richard, B. T. *Int. J. Chem. Kinet.* **1977**, *9*, 133.

(7) Nielsen, O. J.; Johnson, M. S.; Wallington, T. J.; Christensen, L. K.; Platz, J. *Int. J. Chem. Kinet.* **2001**, *34*, 283.

(8) Smith, D. J.; Setser, D. W.; Kim, K. C.; Bogan, D. J. *J. Phys. Chem.* **1977**, *81*, 898.

(9) Atkinson, R.; Baulch, D. L., Cox, R. A.; Crowley, J. N.; Hampson, R. F., Jr.; Kerr, J. A.; Rossi, M. J.; Troe, J. *Summary of Evaluated Kinetic and Photochemical Data for Atmospheric Chemistry*; IUPAC Subcommittee on Gas Kinetic Data Evaluation for Atmospheric Chemistry Web Version, December 2001, 1−56. $k(T) = 1.3 \times 10^{-10}$ (cm^3 $molecule^{-1}$ s^{-1}) exp[(−0.43 ± 0.40 kcal/mol)/*RT*] in the range $T = 180-410$ K.

(10) Frisch, M. J.; Trucks, G. W.; Schlegel, H. B.; Scuseria, G. E.; Robb, M. A.; Cheeseman, J. R.; Montgomery, J. A., Jr.; Vreven, T.; Kudin, K. N.; Burant, J. C.; Millam, J. M.; Iyengar, S. S.; Tomasi, J.; Barone, V.; Mennucci, B.; Cossi, M.; Scalmani, G.; Rega, N.; Petersson, G. A.; Nakatsuji, H.; Hada, M.; Ehara, M.; Toyota, K.; Fukuda, R.; Hasegawa, J.; Ishida, M.; Nakajima, T.; Honda, Y.; Kitao, O.; Nakai, H.; Klene, M.; Li, X.; Knox, J. E.; Hratchian, H. P.; Cross, J. B.; Adamo, C.; Jaramillo, J.; Gomperts, R.; Stratmann, R. E.; Yazyev, O.; Austin, A. J.; Cammi, R.; Pomelli, C.; Ochterski, J. W.; Ayala, P. Y.; Morokuma, K.; Voth, G. A.; Salvador, P.; Dannenberg, J. J.; Zakrzewski, V. G.; Dapprich, S.; Daniels, A. D.; Strain, M. C.; Farkas, O.; Malick, D. K.; Rabuck, A. D.; Raghavachari, K.; Foresman, J. B.; Ortiz, J. V.; Cui, Q.; Baboul, A. G.; Clifford, S.; Cioslowski, J.; Stefanov, B. B.; Liu, G.; Liashenko, A.; Piskorz, P.; Komaromi, I.; Martin, R. L.; Fox, D. J.; Keith, T.; Al-Laham, M. A.; Peng, C. Y.; Nanayakkara, A.; Challacombe, M.; Gill, P. M. W.; Johnson, B.; Chen, W.; Wong, M. W.; Gonzalez, C.; Pople, J. A. *Gaussian03*, revision B.05; Gaussian, Inc.: Pittsburgh, PA, 2003.

(11) Møller, C.; Plesset, M. S. *Phys. Rev.* **1934**, *46*, 618.

(12) Scott, A. P.; Radom, L. *J. Phys. Chem.* **1996**, *100*, 16502.

(13) Curtiss, L. A.; Redfern, P. C.; Raghavachari, K.; Rassolov, V.; Pople, J. A. *J. Chem. Phys.* **1999**, *110*, 4703.

(14) Purvis, G. D.; Bartlett, R. J. *J. Chem. Phys.* **1982**, *76*, 1910.

(15) (a) Hehre, W. J.; Radom, L.; Schleyer, P. v. R.; Pople, J. A. *Ab Initio Molecular Orbital Theory*; Wiley: New York, 1986. (b) Wong, M. W.; Radom, L. *J. Phys. Chem.* **1995**, *99*, 8582.

(16) Wang, B.; Hou, H.; Gu, Y. *J. Phys. Chem. A* **2001**, *105*, 156.

(17) (a) Sander, S. P.; Finlayson-Pitts, B. J.; Friedl, R. R.; Golden, D. M.; Huie, R. E.; Kolb, C. E.; Kurylo, M. J.; Molina, M. J.; Moortgat, G. K.; Orkin, V. L.; Ravishankara, A. R. Chemical Kinetics and Photochemical Data for Use in Atmospheric Studies, Evaluation Number 14, JPL Publication 02-25, Jet Propulsion Laboratory: Pasadena, CA, 2002. (b) Caron, A. S.; Skinner, H. A. *J. Chem. Soc.* **1949**, *201*, 936. (c) Prittchard, H. O.; Skinner, H. A. *J. Chem. Soc.* **1950**, *202*, 1099.

(18) (a) Laidler, K. J. *Chemical Kinetics*, 3rd ed.; Harper and Row: New York, 1987. (b) Berman, M.; Lin, M. C. *J. Phys. Chem.* **1983**, *87*, 3993.

(19) Gonzalez, C.; Schlegel, H. B. *J. Chem. Phys.* **1989**, *90*, 2154.

(20) Ayala, P. Y.; Schlegel, H. B. *J. Chem. Phys.* **1998**, *108*, 2314.

(21) (a) Hegarty, D.; Robb, M. A. *Mol. Phys.* **1979**, *38*, 1795. (b) Yamamoto, N.; Vreven, T.; Robb, M. A.; Frisch, M. J.; Schlegel, H. B. *Chem. Phys. Lett.* **1996**, *250*, 373.